167, 13.9), *Sphyrapicus varius* (149.0, 139 to 168, 8.2), *Xiphorhynchus guttatus* (153.7, 145 to 160, 6.1), *Picoides villosus* (154.4, 146 to 159, 4.1), *Campethera caroli* (156.4, 148 to 164, 5.4), *Picus canus* (160.9, 144 to 170, 8.9), and *Dryocopus pileatus* (161.1, 152 to 174, 7.5).
12. O. Heinroth, *J. Ornithol.* **71**, 277 (1923).
13. P. Brodkorb, in *Avian Biology*, D. S. Farner and J. R. King, Eds. (Academic Press, New York, 1971), vol. 1, pp. 19–54.
14 J. Delacour and D. Amadon, *Currassows and Related Birds* (American Museum of Natural History, New York, 1973).
15. D. W. Yalden, in (*7*), pp. 91–97.
16. O. Mutschler, *Jahresber. Mitt. Oberrheinischen Geol. Ver.* **16**, 25 (1927); K. W. Barthel, N. H. M. Swinburne, S C. Morris, *Solnhofen· A Study in Mesozoic Paleontology* (Cambridge Univ. Press, Cambridge, 1990).
17. S. Tarsitano, in (*7*), pp. 319–332.
18. L. D. Martin, in (*2*), pp. 485–540.
19. M. Sy, *J Ornithol.* **84**, 199 (1936); S. L Olson and A. Feduccia, *Nature* **278**, 247 (1979).
20 A. Feduccia, *The Age of Birds* (Harvard Univ Press, Cambridge, MA, 1980), U. M Norberg, *Vertebrate Flight* (Springer-Verlag, Berlin, 1990)
21 S. Rietschel, in (*7*), pp 251–260.
22 A. Feduccia and H. B. Tordoff, *Science* **203**, 1021 (1979)
23. R. Å. Norberg, in (*7*), pp. 308–318
24. D B. O. Savile, *Evolution* **11**, 212 (1957).
25. D W. Yalden, *Nature* **231**, 127 (1971); *Ibis* **113**, 349 (1971).
26 I thank V. Albert, W. Bock, L. Martin, S. Olson, and S Tarsitano for comments on the manuscript and W. Dickison, P. Gensel, and M Urlichs for paleobotanical advice. V. Albert helped with statistics and Figs. 2 and 3 and S. Tarsitano provided photos for Fig 4. S. Olson provided access to the collections of the U.S National Museum of Natural History. S Whitfield prepared Figs. 1, 5, and 6

11 September 1992; accepted 15 December 1992

A High-Temperature Superconducting Receiver for Nuclear Magnetic Resonance Microscopy

R. D. Black, T. A. Early, P. B. Roemer, O. M. Mueller, A. Mogro-Campero, L. G. Turner, G. A. Johnson

A high-temperature superconducting-receiver system for use in nuclear magnetic resonance (NMR) microscopy is described. The scaling behavior of sources of sample and receiver-coil noise is analyzed, and it is demonstrated that Johnson, or thermal, noise in the receiver coil is the factor that limits resolution. The behavior of superconductors in the environment of an NMR experiment is examined, and a prototypical system for imaging biological specimens is discussed. Preliminary spin-echo images are shown, and the ultimate limits of the signal-to-noise ratio of the probe are investigated.

In high-field (>0.5 T) clinical magnetic-resonance imaging, the patient's body is the main source of experimental noise (*1*) that degrades image quality. As the dimensions of an imaging experiment are reduced (that is, both the specimen and coil are reduced in size), there is a crossover point beyond which the noise of the receiving coil and its associated electronics dominates. The point at which this crossover occurs depends on the strength of the applied magnetic field and on the nuclear spin density of the specimen (*2*). When the specimen no longer dominates the signal-to-noise ratio (SNR) it makes sense to reduce the receiver coil noise, which is thermal (Johnson) noise (*3*), to improve image resolution and reduce data acquisition time (*4*). The Johnson noise power is proportional to the product of resistance and temperature; therefore, reductions in these parameters will have the desired effect. Superconducting materials are clearly attractive candidates for this purpose. This report addresses the details of constructing an NMR imaging probe that incorporates the high-temperature superconductor $Y_1Ba_2Cu_3O_7$ (YBCO).

Table 1 shows how SNR varies with the dimensions of the imaging experiment and with the field strength or, equivalently, the Larmor precessional frequency ω (*5*). The NMR voltage has an r^2 dependence (where r is the linear scale dimension of the sample and receiver coil) owing to the r^3 dependence of spin number on volume and the fact that coil sensitivity goes as r^{-1}. The Bloch equations (*6*) show the origin of the ω^2 dependence. The noise power of the sample is proportional to ω^2 (*7*) and to volume, so the noise voltage of the sample goes as $(\omega^2 r^3)^{1/2}$. The Johnson noise power of the coil is proportional to the resistance R, which is, in turn, proportional to the inverse of the skin depth: skin depth goes as $\omega^{-1/2}$. Therefore, coil noise voltage goes as $\omega^{1/4}$. There is no change in resistance with scaling in the skin depth limit.

To get a physical feeling for the scaling laws, consider a typical experiment at 1.5 T that acquires an image of the human head (*1*). The sample noise power is about ten times that of the coil noise (we neglect noise contributions from the cabling and preamplifier). Shrinking the scale dimension by a factor of ~2 would make the noise powers about equal. If the diameter of the coil around the head is 25 cm, then the coil size at which the noise terms cross is about 12 cm (at 7 T, the scale dimension at which the noise powers become comparable is about 5 cm). Alternatively, if the human head coil stays the same size, the sample and coil noise terms will be comparable when the field is reduced from 1.5 to 0.3 T. It is clear that superconducting head coils designed to work at 1.5 T would not be useful because the patient noise dominates. However, for sample sizes in the range of 1 cm or less in a field of 7 T, a big improvement in SNR can be achieved if we reduce the coil noise.

Two principal issues complicate the use of superconducting materials in NMR imaging. Superconductors revert to the normal, nonsuperconducting state in sufficiently high magnetic fields and at large enough temperatures. None of the elemental superconductors (such as Nb or Pb) can withstand the 7-T field or the 10 K operating temperature that exists in the system described below. The A-15 materials (for example, Nb_3Sn and Nb_3Al) have critical parameter values that are large enough, but tests of the Nb_3Al film resonators that we constructed showed them to have lower quality factors than the YBCO film resonators that we made. The extremely high critical temperature and the critical field values of YBCO films make them the best choice.

The YBCO films were produced by co-evaporation and post-annealing procedures that are described elsewhere (*8*). The 0.6-μm-thick films were deposited onto both sides of a 0.5-mm-thick, 2.5-cm-diameter $LaAlO_3$ substrate. We chose $LaAlO_3$ for its crystallographic compatibility with YBCO and its relatively low dielectric loss tangent. The films were patterned with the use of conventional photolithographic techniques and were etched with 0.01 N nitric acid. The YBCO was patterned into a split ring shape (18-mm outer and 14-mm inner di-

Table 1. Scaling laws for NMR imaging. The frequency ω is proportional to magnetic field strength. The linear scale size of the sample and coil is represented by r. One can determine the constant A empirically by measuring the sample and coil losses for head images at 1.5 T. When the coil is cooled, its voltage noise will decrease by a factor equal to the square root of the ratio of the coil temperature to the sample temperature. SNR is signal-to-noise ratio.

NMR voltage	$\omega^2 r^2$
Sample noise voltage	$\omega r^{3/2}$
Coil noise voltage	$\omega^{1/4}$
Intrinsic SNR (sample)	$\omega r^{1/2}$
SNR (coil + sample)	$\dfrac{\omega^2 r^2}{\sqrt{\omega^2 r^3 + A\omega^{1/2}}}$
Imaging time	$1/(\mathrm{SNR})^2$

R. D Black, T. A. Early, P B. Roemer, O M. Mueller, A. Mogro-Campero, L. G Turner, General Electric Corporate Research and Development Center, Schenectady, NY 12301.
G. A. Johnson, Departments of Radiology and Physics, Duke University, Durham, NC 27710.

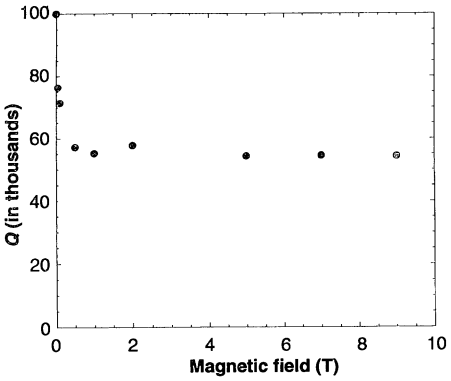

Fig. 1. Plot of Q versus magnetic field strength for a YBCO resonator at 4.2 K. The field was applied along the *a–b* plane.

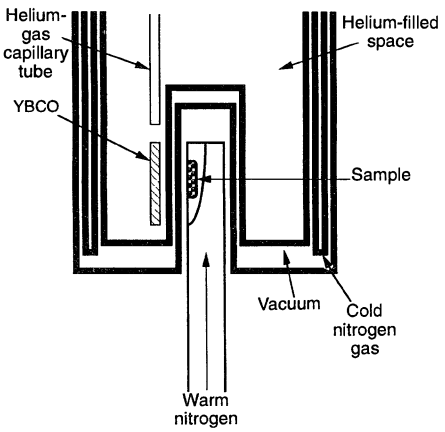

Fig. 2. Lower portion of the quartz dewar that holds the YBCO resonator (not drawn to scale for sake of clarity). Fixed-temperature helium gas is blown onto the resonator from a capillary tube. The sample is kept at room temperature by warm nitrogen gas. Cold nitrogen gas flows in a narrow space near the outer wall. The total separation between the helium space and the sample space is 3 mm and the sample space is 1 cm across.

ameter) on each side of the substrate (9). The gaps in the rings were diametrically opposed, and the resulting LC (inductive/capacitive) structure resonated at 300 MHz (the Larmor frequency for protons at 7 T).

The Qs (quality factor) of the resonators were measured with a Hewlett-Packard 8568A spectrum analyzer and a sweep generator. Each resonator was placed in a variable field produced by a superconducting magnet (Janis Research Supervaritemp dewar with a Cryomagnetics 9-T magnet), and the value of Q was recorded as a function of field strength and temperature. All measurements were performed with the field approximately parallel to the *a–b* plane of the YBCO (parallel to the substrate). There was a large initial drop in Q as the field was increased (Fig. 1). This was most likely the result of the rapid influx of quantized magnetic flux vortices (fluxons) as the lower critical field of the YBCO was exceeded. After this initial drop, Q did not change significantly with field up to 9 T. Therefore, Q was around 50,000 at 7 T, the field at which the microscopy system described herein operates.

For a series resonant circuit, $Q = \omega L/R$. A high Q leads to reduced Johnson noise as a result of the R dependence of the noise power. For the case in which coil noise dominates, we have

$$\mathrm{SNR} \propto \sqrt{\frac{Q}{T}} \qquad (1)$$

where T is absolute temperature. A copper resonator that is the same size as the YBCO resonator has a Q value of about 400 at room temperature (*9*, *10*). Therefore, the use of a YBCO coil at 10 K will yield an SNR gain of ~60 relative to such a copper coil.

This gain can be used to decrease the imaging time by a factor of 3600. In practice, the imaging time reduction will be limited by the relaxation times (T_1 and T_2) of the spin system. However, there are certain fast-scanning techniques (*11*) that can increase the rate of data acquisition when the SNR is sufficiently large. The gain can also be used to decrease the linear dimensions of the smallest volume element that is imaged (a voxel) by a factor of ~4. Potential limits on the resolution are posed by a number of factors, including susceptibility (*12*), inherent linewidth (*13*, *14*), and diffusion (*15–19*). To date, a meaningful experimental verification of these limits has not been possible because of the resolution limits imposed by low SNR. The superconducting receiver should allow for a practical study of these limits.

Care must be taken to ensure that specimens to be imaged can be maintained at room temperature while the YBCO resonator, sitting in close proximity, stays at 10 K. This was accomplished with the dewar design shown in Fig. 2. The dewar was constructed entirely of quartz, and cooling was accomplished with helium and nitrogen gases to avoid vibration caused by bubbling. Nitrogen gas passed through a coil that was immersed in liquid nitrogen and then flowed into the nitrogen space where it cooled the outer walls. Helium gas was delivered through a valved capillary transfer tube to a heating block within the dewar. A Lakeshore 82C temperature controller warmed the gas to a preset temperature as it flowed down a quartz capillary tube and onto the YBCO resonator. The resonant frequency is temperature-dependent, which means accurate control was essential: the high Q of the resonator makes it very susceptible to frequency drift. The total thickness of the quartz walls and vacuum gap that separated the resonator from the sample was 3 mm. Samples were held in a pocket on the inner wall of a quartz tube through which warm nitrogen flowed. This arrangement allowed for the samples to be maintained at room temperature and still be kept less than 5 mm from the resonator.

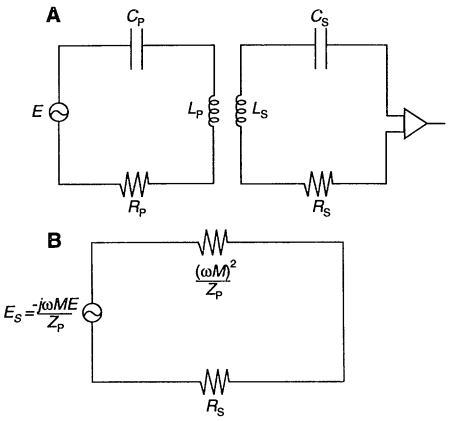

Fig. 3. (**A**) The circuit diagram for the inductively coupled YBCO resonator (p, primary) and the room-temperature copper resonator (s, secondary) and (**B**) the equivalent circuit for the secondary at resonance.

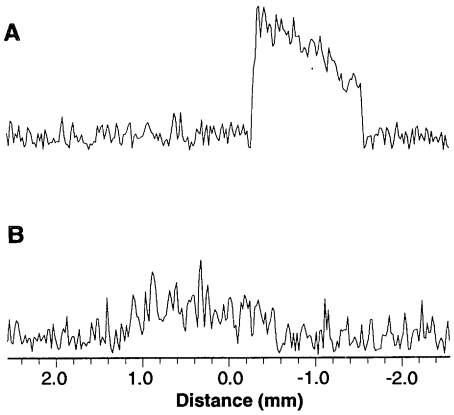

Fig. 4. SNR profiles (dimensionless) for (**A**) the high-temperature superconducting (HTS) probe (SNR ~11 to 12) and (**B**) the room-temperature copper solenoid (SNR ≥1). These are line plots (256 pixels) through single slices of the three-dimensional data. The height of the profile in the sample region (high signal region) relative to the baseline (noise) gives SNR.

To achieve the SNR gains that were calculated above, it is necessary to couple to the superconducting resonator in a way that does not add significant noise. There is a straightforward inductive coupling approach that makes this possible (Fig. 3A). The superconducting resonator is represented as the primary circuit, and the voltage E is the induced NMR voltage. At resonance, the inductive and capacitive reactances cancel out, and the impedance is simply the real resistance R_p (*20*). The secondary circuit consists of a room-temperature copper loop and a low loss capacitor. There is a mutual inductance M between the two resonant

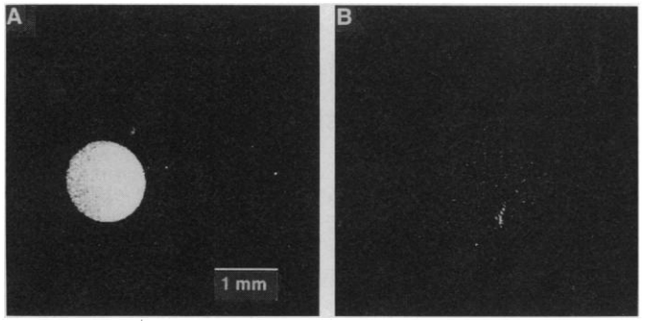

Fig. 5. Single slice images (the two images from the data used for Fig. 4 that yielded the highest contrast) taken with (**A**) the HTS probe and (**B**) the room-temperature copper solenoid. To facilitate comparison, the background levels were adjusted to be equal. The different cross sections were a result of the sample tube being in a different orientation for the two probes.

circuits. Solving the loop equations for the two circuits leads to the equivalent circuit for the secondary shown in Fig. 3B (*21*). The effective impedance of the primary as seen in the secondary is $(\omega M)^2/Z_p$, and $Z_p = R_p$ at resonance. By adjusting the relative positions of the two resonators, M can be made large enough that this effective impedance term dominates other impedance terms in the secondary (*22*). Typically, the effective impedance is set to 50 ohms and R_s can be made to be a few tenths of an ohm (the inductive and capacitive reactances in the secondary cancel at resonance). One must be careful to note, however, that the noise power of the effective impedance will be that of a 50-ohm resistor at 10 K.

The SNR of the primary circuit alone (at resonance) is

$$\mathrm{SNR} \propto \frac{E}{\sqrt{R_p}} \qquad (2)$$

The SNR for the equivalent secondary circuit (Fig. 3B) is

$$\mathrm{SNR} \propto \frac{\omega ME}{R_p}\left[\frac{(\omega M)^2}{R_p}\right]^{-\frac{1}{2}} = \frac{E}{\sqrt{R_p}} \qquad (3)$$

Even though the net Q of the two circuits must be lower than that of the superconducting circuit alone, the SNR gain is preserved as long as the effective impedance term dominates the other impedance terms in the equivalent secondary circuit.

To keep the noise of the entire receiver chain low, it is necessary to have a low noise preamplifier. Common source configuration preamplifiers containing GaAs MESFETs (metal–semiconductor field–effect transistors) from several different manufacturers have been constructed (*23*). The small values of the capacitance between the gate and the source (0.3 to 0.5 pF) determine the optimum source impedance of the FETs (1000 to 3000 ohms). The key to achieving low noise lies in providing an impedance transformation network that has a high Q. Large air core inductors and low loss variable capacitors are used to achieve this. The preamplifier is tuned to have a noise minimum at the Larmor frequency (300.5 MHz for protons at 7 T). Cooling the amplifier in liquid nitrogen causes a significant drop in noise temperature, and it is believed that the remaining dominant noise source is the Johnson noise of the input transformer. Careful design has resulted in preamplifiers that have noise temperatures of 10 K when cooled to 77 K.

We have performed conventional spin-echo experiments with a 300-MHz GE Omega imaging system to compare the superconducting probe with a 4-mm-diameter, room-temperature copper solenoid. The same phantom composed of $CuSO_4$ in water (2 g/liter) was imaged with the two coils. The copper solenoid had a geometric coupling advantage, as compared with the high-temperature superconducting (HTS) coil, owing to its larger filling factor. Both probes were run with the same acquisition parameters: 200-ms recovery time, 22-ms echo time, 5.12 mm by 5.12 mm by 0.32 mm field of view, two averages, 256 by 256 by 16 matrix size. This resulted in a 27-min acquisition time and a 20 μm by 20 μm by 20 μm voxel size. The GaAs-FET preamplifier was not cooled in these runs; therefore, the total noise temperature of the receiver chain was about 85 K (the same amplifier was used for the two probes). We saw an improvement in the SNR by a factor of ~10 (Fig. 4) with the HTS probe in spite of the geometric coupling advantage of the copper solenoid. Comparative images are shown in Fig. 5.

The superconducting probe has a significant SNR advantage over conventional probes. Use of the SNR gain to reduce imaging time would be a very powerful development for histopathologic studies (*24, 25*), in which extreme resolution is not the main goal. Moreover, the ability to probe the limits of resolution with a relatively large sample (*26, 27*) will make possible new structural and functional studies. There are interesting prospects for applying this same technology to NMR spectroscopy studies for situations in which signal levels are marginal.

REFERENCES AND NOTES

1. W. A. Edelstein, G. H. Glover, C. J. Hardy, R. W. Redington, *Magn. Reson. Med.* **3**, 604 (1986).
2. We shall discuss proton imaging only.
3. J. B. Johnson, *Phys. Rev.* **32**, 97 (1928).
4. P. Styles, N. F. Soffe, C. A. Scott, *J. Magn. Reson.* **84**, 376 (1989).
5. R. D. Black *et al.*, in *Proceedings of the Tenth Annual Meeting of the Society of Magnetic Resonance in Medicine*, San Francisco, CA, 10 to 16 August 1991, E. R. Andrew, Ed. (Society of Magnetic Resonance in Medicine, Berkeley, CA, 1991), p. 1250.
6. F. Bloch, W. W. Hansen, M. E. Packard, *Phys. Rev.* **69**, 127 (1946).
7. D. I. Hoult and P. C. Lauterbur, *J. Magn. Reson.* **34**, 425 (1979).
8. A. Mogro-Campero and L. G. Turner, *Appl. Phys. Lett.* **58**, 417 (1991).
9. M. B. Banson, G. P. Cofer, R. D. Black, G. A. Johnson, *Invest. Radiol.* **27**, 157 (1992).
10. Of the thin-film copper coils of the same size that we have tested, none have had a Q larger than 2000 at 4.2 K. This is primarily due to the much higher sheet resistance of copper at 300 MHz, even at the temperature of liquid helium [see G. Muller *et al.*, *J. Supercond.* **3**, 235 (1990)]; but it also depends on film quality, impurity levels in the copper, and current crowding effects. For copper wire resonators with discrete capacitors, the Q of the capacitor can be dominant and may limit the resonator Q to a value lower than that allowed by the copper.
11. M. K. Stehling, R. Turner, P. Mansfield, *Science* **254**, 43 (1991).
12. P. T. Callaghan, *J. Magn. Reson.* **87**, 304 (1990).
13. C. D. Eccles and P. T. Callaghan, *ibid.* **68**, 393 (1986).
14. W. V. House, *IEEE Trans. Nucl. Sci.* **NS31**, 570 (1984).
15. P. Mansfield and P. K. Grannell, *Phys. Rev. B* **12**, 3618 (1975).
16. P. T. Callaghan and C. D. Eccles, *J. Magn. Reson.* **78**, 1 (1988).
17. Z. H. Cho *et al.*, *Med. Phys.* **15**, 815 (1988).
18. C. B. Ahn and Z. H. Cho, *ibid.* **16**, 22 (1989).
19. E. W. McFarland, *Magn. Reson. Imaging* **10**, 269 (1992).
20. The resistance R is only truly zero for dc current. At any finite temperature, there is a residual number of quasiparticles that are not in the superconducting state, and they contribute to ac resistance.
21. F. E. Terman, *Radio Engineers' Handbook* (McGraw-Hill, New York, 1943), p. 148.
22. Viewed differently, the transformer formed by the two resonators increases the induced voltage in the secondary relative to that in the primary. Also, the current needed to cause a 90° spin flip is small because the transformer increases the current of the transmitted radio frequency (RF) pulse.
23. O. M. Mueller and W. A. Edelstein, in *Proceedings of the Sixth Annual Meeting of the Society of Magnetic Resonance in Medicine*, New York, 17 to 21 August 1987, E. R. Andrew, Ed. (Society of Magnetic Resonance in Medicine, Berkeley, CA, 1987), p. 411.
24. G. A. Johnson, M. B. Thompson, G. P. Cofer, D. Campen, R. R. Maronpot, *Vet. Pathol.* **26**, 303 (1989).
25. G. A. Johnson, R. R. Maronpot, R. W. Redington, *Invest. Radiol.* **25**, 1361 (1990).
26. All extremely high-resolution imaging (voxels less than 10 μm per side) is performed with small coils that are tightly coupled physically to the sample. This limits the field of view and access to information on extended three-dimensional structures.
27. E. W. McFarland and A. Mortara, *Magn. Reson. Imaging* **10**, 279 (1992).

28. We acknowledge the technical assistance of D. W. Lillie, P. J. Bednarczyk, C. J. Rossi, D. W. Skelly, K. W. Rohling, J. W. Bray, and W. A. Edelstein and the managerial support of W. L. Robb and R. W. Redington. Support at the Center for In Vivo Microscopy, Duke University Medical Center, was received under NIH 1P41 RR05959, NIH ES0 4187, and NSF CDR 862 2201.

27 August 1992; accepted 25 November 1992